How to Understand and Interpret Current Flow in Nanopore/Electrode Devices

Tim Albrecht*

Department of Chemistry, Imperial College London, Exhibition Road, London SW7 2AZ, U.K.

ABSTRACT Nanopore-based single-molecule sensors have become an important class of analytical devices that have in some cases already reached the market place. Traditionally operated in a two-electrode configuration, devices with three or more electrodes have emerged recently, for example with a view on switching the transport properties of the nanopore or even tunneling-based detection of analytes with the ultimate goal of inexpensive and ultrafast DNA sequencing. How do these additional electrodes affect the current distribution in the cell and hence the sensor performance? This is significantly less clear and thus in focus here. We use impedance modeling of a prototypical three-electrode nanopore sensor and show that, depending on the conditions, standard experimental device characterization is severely affected by the presence of the third electrode. On the other hand, the simulations also provide guidelines on how to avoid such complications, identify "safe" operating conditions, and design criteria for optimized nanopore sensors.

KEYWORDS: single-molecule · sensing · sequencing · solid-state · nanopore

Nanopore devices have developed into an important class of single-molecule (bio)sensors. These include both biological pores—typically embedded in a lipid bilayer—and "solid-state" nanopores, where the membrane material is made of a highly insulating, solid material, such as Si_3N_4, SiO_2, polymers, or graphene.[1−17] The capabilities of nanopore-based biosensors may even extend to ultrafast, inexpensive and label-free DNA or RNA sequencing, which has been a major driving force in this area for many years.[18−21]

The operating principle of a nanopore device is relatively simple. It consists of a liquid cell, which is separated into two compartments by the thin membrane. The latter encompasses a small aperture, the nanopore, which is the only connection for ions and fluid to be transferred between the two compartments. Moreover, each compartment typically contains one electrode, which is in rapid redox equilibrium with the surrounding electrolyte, for example, AgCl-coated Ag electrodes immersed in a chloride-containing electrolyte. For small pores, say with diameters smaller than 100 nm, the nanopore resistance R_{pore} is usually much larger than the solution resistance R_s. Hence, upon application of a constant voltage E, an ion current I_{ion} is induced that depends on the cross-sectional area and length of the pore channel, the conductivity of the electrolyte, and for very small pores also to a significant extent on the surface charge density inside the pore.[22] The majority of the potential E thus drops at the nanopore, creating a relatively strong electric field on the order of about 10^6 V/m. It is the electric field that is the major driving for the translocation of charged biomolecules, such DNA, RNA, or proteins.

Since a well-prepared Ag/AgCl electrode is very close to an ideal nonpolarizable electrode, there is negligible capacitive charging and hence only a very small (and constant) potential drop at the electrode/solution interface. Equivalently, the definition of an ideal nonpolarizable electrode implies fast interfacial redox kinetics or a low (ideally zero) charge transfer resistance R_{ct}. Hence, a relatively simple electric equivalent circuit can be used to capture the main impedance characteristics of the device, which includes a solution resistance R_s, an effective membrane capacitance C_{mem} and the pore resistance R_{pore}.

On the other hand, if ideal polarizable electrodes were used, $R_{ct} \rightarrow \infty$, no charge could be transferred across the electrode/solution interface and hence no steady-state current could be maintained. As a consequence, the voltage E would drop exclusively at the electrode/solution interfaces. The potential drop in solution including the nanopore is then zero (provided the electrolyte concentrations are the same in both compartments). In reality, any electrode used is in between these two limiting cases depending on the nature and size of the electrode, the solution conditions, and the applied potential.

The situation becomes more complicated when more electrodes are introduced into

* Address correspondence to t.albrecht@imperial.ac.uk.

Received for review June 18, 2011 and accepted July 26, 2011.

Published online July 26, 2011
10.1021/nn202253z

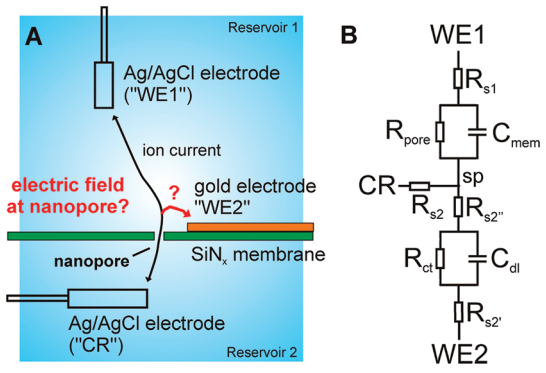

Figure 1. (A) Electrochemical setup including liquid cell. The nanopore membrane separates two reservoirs, 1+ 2, filled with electrolyte. Ion or liquid transport between the reservoirs is only possible *via* the nanopore. (B) Electric equivalent circuit model. R_{s1}, R_{s2}, $R_{s2'}$, $R_{s2''}$, R_{pore}: solution and nanopore resistances, respectively. C_{mem} = capacitance associated with the siliconnitride membrane; C_{dl}, R_{ct} = double layer capacitance and charge transfer resistance related to WE2; "sp" indicates a summing point (see text for further details).

the system, for example, when using electrically conductive (switchable or gated) nanopores[23−26] or integrating a tunnelling junction with the nanopore with potential applications in ultrafast, label-free DNA or RNA sequencing.[27−31] Importantly, these additional electrodes may have quite different interfacial properties ranging from the ideal nonpolarizable ($R_{ct} \rightarrow 0$) to the perfectly polarizable regime ($R_{ct} \rightarrow \infty$).

Since the current distribution in the nanopore device and hence the potential drop at the nanopore depend on the charge transfer properties of all electrodes present in the system, it is important to understand their mutual influence, in order to control the electric field across the membrane and thus the translocation of biomolecules during sensing or sequencing operation. While the effect of electrode charge on the pore translocation characteristics has been studied in quite some detail (essentially representing the $R_{ct} \rightarrow \infty$ case),[9,32−36] less attention has apparently been paid to Faradaic effects, namely charge transfer at the various electrodes and its effect on the electric driving field at the pore.

In this paper, current/voltage relationships for the most relevant experimental scenarios in a three-electrode nanopore device are derived based on a simple impedance model, Figure 1A/B. Focus will be in particular on the role of the third electrode and its ability to draw (or supply) current; its charge transfer resistance R_{ct} can generally vary from very large to close-to-zero. The other two electrodes will be taken as perfectly nonpolarizable electrodes, in close analogy to a typical nanopore sensor.

While details of the equivalent circuit *inter alia* depend on the actual design of the nanopore sensor and may vary from the circuit used here, the current model can easily be adapted. The general approach and main qualitative conclusions hold regardless: namely that the main operating parameters, such as the electric field across the nanopore membrane, the time response of the cell, and the general performance of the device critically depend upon the charge transfer characteristics of the third electrode WE2.

Current−time and current−voltage dependences will be derived for the most relevant modulation schemes, namely for constant potentials of WE1 and WE2, E_{1CR} and E_{2CR}, potential steps in E_{1CR} or E_{2CR}, for linear ramping of E_{1CR} or E_{2CR}, for sinusoidal potential modulations. One comment regarding the nomenclature: It has been chosen to reflect as much information in each parameter as possible while minimizing their complexity. For example, E_{1CR} refers to the potential difference between working electrode 1 and the combined counter and reference electrode "CR", $E_{1CR} = E_1 - E_{CR}$. The amplitude of a potential modulation of E_{1CR} is then labeled ΔE_{1CR} and so forth (see below). A tilde on top of a parameter indicates that it is treated in Laplace space. Moreover, a number of important special cases will be discussed, for example when the pore resistance R_{pore} changes with time—as experimentally investigated by Ayub *et al.*[23]—and when the charge transfer characteristics of WE2 vary with E_{2CR}.

HOW DOES THE CURRENT FLOW? THE UNDERLYING MODEL

Figure 1A shows a typical experimental configuration for a nanopore sensor device with more than two electrodes.[23,24] The siliconnitride membrane (green, "SiN_x" if nonstochiometric) with the nanopore separates the upper and lower compartments of the electrochemical cell (reservoirs 1 and 2). Both CR and WE1 are ideal nonpolarizable electrodes, for example (ideal) Ag/AgCl electrodes in a chloride-containing electrolyte ($R_{ct} \rightarrow 0$). On the other hand, WE2 may be a metal (*e.g.*, Au) electrode either somewhere in the solution of reservoir 2 or deposited onto the Si_3N_4 membrane. Accordingly, R_{ct} may vary from effectively zero to very large values.

To illustrate the rationale behind this circuit, we shall assume that oxidation only takes place at WE1, which is counterbalanced by reduction at CR and WE2. The current flowing from WE1 into the cell passes through the nanopore and is then formally "split" between CR and WE2. In the circuit diagram, we represent this point as a summing point sp. Physically, sp is located where the solution resistance measured between CR and WE1, CR and WE2, and WE1 and WE2 is equal to $(R_{s1} + R_{s2} + R_{s2''})$, $(R_{s2} + R_{s2'})$ and $(R_{s1} + R_{s2'} + R_{s2''})$, respectively.

At first sight, this may appear overparameterized, but it allows for sp to be uniquely defined both electrically and in terms of its physical location in the cell. Note that the solution resistances are important,

particularly for small R_{ct} and large E_{2CR}, for defining the potential drop E_{1sp} and the current I_{1sp} detected at WE1. Further details regarding the mathematical derivations are given in the Methods section. The two key equations for the potential drop across the membrane E_{1sp} and the current detected at WE1, I_{1sp}, are

$$\tilde{E}_{1sp} = \left[1 - \frac{Y_{asp}}{Y_{spCR} + Y_{1sp} + Y_{2sp}}\right]\tilde{E}_{1CR} - \frac{Y_{2sp}}{Y_{spCR} + Y_{1sp} + Y_{2sp}}\tilde{E}_{2CR} \quad (1)$$

and

$$\tilde{I}_{1sp} = \left[1 - \frac{Y_{asp}}{Y_{spCR} + Y_{1sp} + Y_{2sp}}\right]\tilde{E}_{1CR} - \frac{Y_{2sp}}{Y_{spCR} + Y_{1sp} + Y_{2sp}}\tilde{E}_{2CR} \quad (2)$$

RESULTS AND DISCUSSION

Starting with Simplest Case: The Steady-State Pore Current at Constant Potentials. *Typical Scenario.* A metallic or metal-coated nanopore is used as a gating device. Applying a potential to the membrane electrode allows control of the electrochemical reactivity, the surface charge, and modulation of the transport characteristics.[23,25] Similar devices are also used for optical detection of DNA translocation (zero-mode waveguide technology),[37] where currents across the membrane can cause corrosion of the metal layer in the proximity of the pore.[24]

For the input functions to eq 1, we have in Laplace space $\tilde{E}_{1CR} = E_{1CR}/s$ and $\tilde{E}_{2CR} = E_{2CR}/s$. After solving eq 2 and the inverse Laplace transform, we neglect any transient behavior of $I_{1sp}(t)$ at short times for now, and obtain an expression for $I_{1sp}(t)$ under steady-state conditions:

$$I_{1sp}(t)_{ss} = \frac{R_{ct} + 2R_s}{(R_{ct} + 2R_s)R_{pore} + 5R_s^2 + 3R_sR_{ct}}E_{1CR} - \frac{R_s}{(R_{ct} + 2R_s)R_{pore} + 5R_s^2 + 3R_sR_{ct}}E_{2CR} \quad (3)$$

For the two limiting cases of R_{ct}, *viz.* $R_{ct} \to \infty$ and $R_{ct} = 0$, taking $R_{pore} \gg R_s$, this yields

$$I_{asp}(t)_{ss} = \frac{1}{R_{pore}}E_{1CR} \quad (\text{for } R_{ct} \to \infty) \quad (3a)$$

and

$$I_{asp}(t)_{ss} = \frac{1}{R_{pore}}E_{1CR} - \frac{1}{2R_{pore}}E_{2CR} \quad (\text{for} R_{ct} = 0) \quad (3b)$$

This is in line with expectations in that a perfectly polarizable electrode does not draw any current in steady-state and hence does not affect the current distribution in the cell. Any electrostatic charge on electrode surface is screened after a few Debye lengths, depending on the ionic strength of the solution after *ca.* 1−10 nm. On the other hand, a perfectly polarizable electrode does draw significant currents, even at long times. The potential E_{2CR} drops partly toward sp, altering the effective electric field at the nanopore, *cf.* above. This may lead to a zero net current and even inversion of the current $I_{1sp}(E_{1sp}, E_{2sp})$, as illustrated in Figure 2.

In panel A ($R_{ct} \to \infty$), I_{1sp} is independent of E_{2CR} and the contour lines run in parallel to the E_{2CR}-axis. However, it is linearly dependent on E_{1CR}, varying from −5 to +5 nA based on the parameters used.

By contrast, in case B ($R_{ct} = 0$), I_{1sp} depends linearly on both E_{1CR} and E_{2CR}; the contour lines have a slope of 2, as can be easily confirmed with eq 3b setting $I_{1sp}(t)_{ss} = 0$. The diagonal running through $E_{1CR} = E_{2CR} = 0$ V represents the boundary between positive and negative currents, illustrating that even for $E_{1CR} > 0$, $I_{1sp} < 0$ for large enough E_{2sp} (and equivalently the opposite relations). E_{1sp} is a superposition of E_{1CR} and E_{spCR} and hence I_{1sp} can be larger than for case shown in Figure 2A.

Main Conclusions. The pore conductance G_{pore} can no longer be calculated easily from the pore current and the applied bias, as in a two-electrode setup, unless the R_{ct} associated with WE2 is known (or $R_{ct} \to \infty$). The corresponding current sources need not be an electrode, whose potential is actively controlled: Any electrochemically active surface undergoing a Faradaic reaction under given solution conditions (*e.g.*, dissolution or corrosion) will contribute to the overall current distribution in the cell and thus affect the electric field at the nanopore.

Local Switching of Nanopore Properties: A Potential Step at WE2. This scenario applies when the potential of WE2 is switched in a stepwise fashion, for example to rapidly alter the pore charge during translocation.

In this case, $\tilde{E}_{1CR} = E_{1CR}/s$ and $\tilde{E}_{2CR} = E_{2CR}/s$, as in Figure 2A, but now the time-dependent components in the inverse Laplace transform can no longer be ignored for E_{2CR}. Those for E_{1CR} have vanished by the time WE2 is switched, since E_{1CR} is taken to be constant throughout. The current I_{1sp} is then approximately:

$$I_{1sp}(t) \approx \frac{R_{ct} + 2R_s}{A_2}E_{1CR} - \frac{R_s}{A_2}E_{2CR} + R_sE_{2CR}\left\{\left(\frac{1}{5R_s^2}A_1 - 2K_2\right)(4A_0A_2 - A_1^2)^{-1/2} \times \sin\left(\frac{(4A_0A_2 - A_1^2)^{1/2}}{2A_0}t\right) - \frac{1}{5R_s^2}\cos\left(\frac{(4A_0A_2 - A_1^2)^{1/2}}{2A_0}t\right)\right\}\exp\left(-\frac{A_1}{2A_0}t\right) \quad (4)$$

where $K_1 = R_{ct}C_{dl}$, $K_2 = R_{pore}C_{mem}$, and

$$A_0 = 5R_s^2K_1K_2$$

$$A_1 = (K_1 + K_2)5R_s^2 + (2R_{pore}K_1 + 3R_{ct}K_2)R_s$$

$$A_2 = (R_{ct} + 2R_s)R_{pore} + (5R_s + 3R_{ct})R_s$$

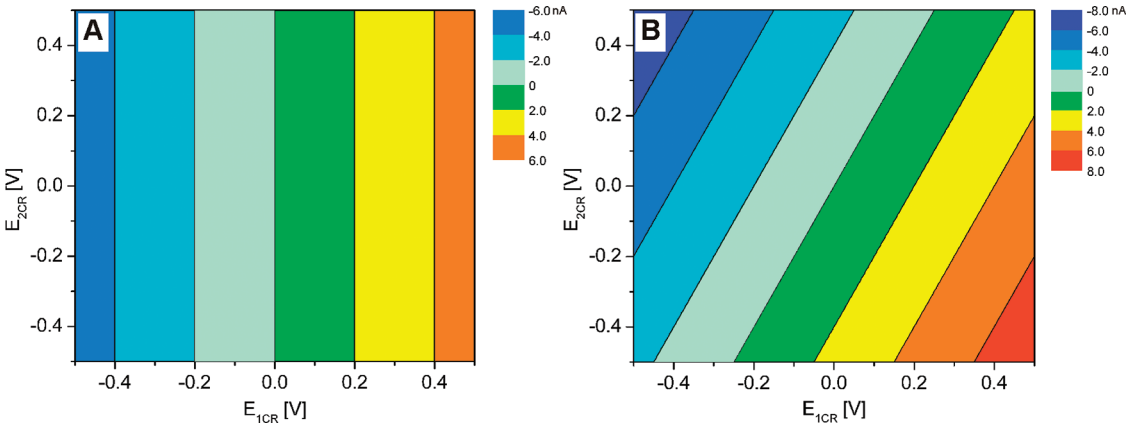

Figure 2. Contour plots of $I_{1sp}(E_{1CR}, E_{2CR})$, according to eqs 3a and 3b. R_{pore} = 100 MΩ, R_s = 100 Ω; the color scale is defined in nA from −6 to +6 nA for panel A and −8 to +8 nA for panel B, respectively. (A) $R_{ct} \rightarrow \infty$ (perfectly polarizable electrode WE2), (B) R_{ct} = 0 (perfectly nonpolarizable electrode WE2). Note that each color corresponds to a current range and not to a constant current value (which are represented by the contour lines).

Again, for $t \gg t_0$, the exponential term in eq 4 approaches zero and the steady-state limit is recovered, eq 3. The characteristic decay time $\tau = (A_1/2A_0)^{-1}$ is

$$\tau = \frac{10R_s(R_{ct}c_{dt})(R_{pore}c_{mem})}{(5R_s + 2R_{pore})R_{ct}c_{dl} + (5R_s + 3R_{ct})R_{pore}c_{mem}} \quad (5)$$

which, for R_{pore}, $R_{ct} \gg R_s$ and $C_{dl} \gg C_{mem}$, simplifies to

$$\tau \approx 5R_sC_{mem}$$

The current I_{1sp} at the beginning of the potential step is given by

$$I_{1sp}(t_0) = \frac{R_{ct} + 2R_s}{(R_{ct} + 2R_s)R_{pore} + 5R_s^2 + 3R_sR_{ct}}E_{1CR} - \left(\frac{R_s}{(R_{ct} + 2R_s)R_{pore} + 5R_s^2 + 3R_sR_{ct}} + \frac{1}{5R_s}\right)E_{2CR} \approx \frac{1}{R_{pore}}E_{1CR} - \frac{1}{5R_s}E_{2CR} \quad \text{for } R_{pore} \gg R_{ct}, R_s \quad (6)$$

Equation 6 suggests that, given E_{1CR} and E_{2CR}, $I_{1sp}(t_0)$ can be both positive and negative, depending on R_{pore}. The critical pore resistance R_{pore} at $I_{1sp}(t_0 = 0)$ is given by

$$R_{pore}^{crit} = 5R_s\frac{E_{1CR}}{E_{2CR}} - R_s\frac{3R_{ct} + 5R_s}{R_{ct} + 2R_s} \quad (7)$$

and is on the order of several R_s, if $E_{1CR} \approx E_{2CR}$. Interestingly, similar behavior was indeed observed experimentally,[23] even though those experiments also involved an electroactive species, complicating a quantitative comparison with eq 3. This will be discussed in more detail below.

Main Conclusions. In general, the characteristics of the $I_{1sp}(t)$ trace will depend on all elements of the equivalent circuit above, which is illustrated in Figure 3. Even the qualitative shape of the $I_{1sp}(t)$ curve depends on the relative magnitudes of R_{pore}, R_{ct}, C_{mem}, and C_{dl}. The initial $I_{1sp}(t = t_0)$ can be negative, positive, or zero, depending on R_{pore}. The characteristic decay time depends on R_s and C_{mem}, if both R_{pore} and R_{ct} are sufficiently large.

Triggering Electrochemical Reactions at the Nanopore. This scenario refers to switching the potential of WE2, in order to induce an electrochemical (Faradaic) reaction at WE2, for example in generating electroactive species at the nanopore or for electrodeposition. The latter was exploited previously in the fabrication of metallic nanopores using real-time ion current feedback.[23]

As the electrodeposition process occurs, both the length L_{pore} and diameter d_{pore} of the nanopore change, resulting in an overall increase of R_{pore} over time. For a given deposition rate a, $L_{pore}(t) = L_{pore,0} + at$, and $d_{pore}(t) = d_{pore,0} - at$. For an uncharged pore, R_{pore} is then simply given by

$$R_{pore}(t) = \frac{4(L_{pore} + at)}{\pi(d_{pore} - at)^2}\rho \quad (8)$$

ρ is the resistivity of the solution. Further complexity could be added to this expression, for example a surface term for charged pores.[22] This decreases R_{pore} for small d_{pore}, but does not add anything qualitatively new to the present discussion and shall thus be ignored here.

Using eq 8 in eq 4 and taking R_{ct}, C_{mem}, and C_{dl} to be constant, the effect of a decreasing R_{pore} on the transient behavior of I_{1sp} is shown in Figure 4 for two different initial values of d_{pore} = 100 nm (black, solid) and 50 nm (red, dashed), respectively (a = 100 nm/s, L_{pore} = 300 nm, ρ = 0.775 Ω^{-1} m^{-1} (0.1 M KCl), R_{ct} = 10 KΩ, C_{dl} = 23.8 μF, C_{mem} = 12.2 μF).

The result is very similar to the experimental data obtained in Ayub *et al.*,[23] lending support to the validity of the model used here. However, it should also be noted that in conjunction with eqs 3a and 3b, the relation between I_{1sp} and R_{pore} (and hence its geometry) is only trivial for large R_{ct}. In all other cases, details of the potential distribution between CR and WE2 as well as E_{2CR} must be known, rendering absolute

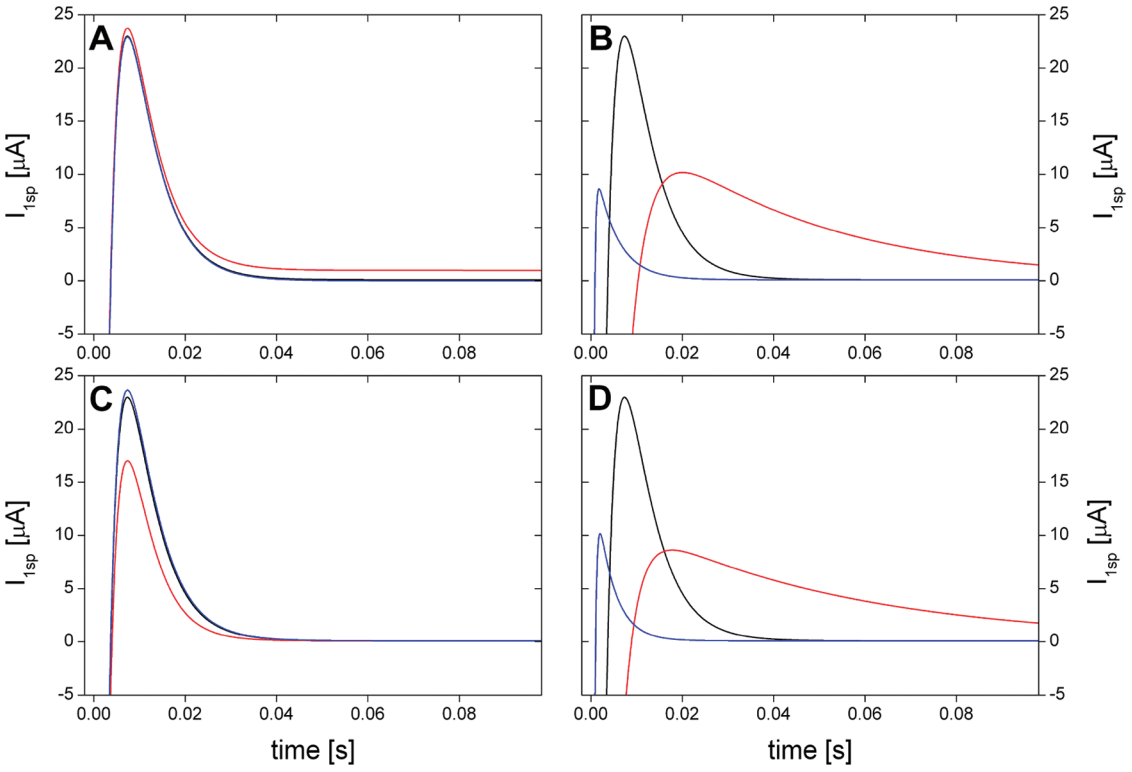

Figure 3. Current−time profiles for I_{1sp} after a potential step in E_{2CR} from 0 to 0.1 V (E_{1CR} = 0.1 V = constant, R_s = 100 Ω). (A) C_{mem} = 12.2 μF, R_{ct} = 10 KΩ, C_{dl} = 23.8 μF; (black) R_{pore} = 1 MΩ, (red) R_{pore} = 100 KΩ, (blue) R_{pore} = 10 MΩ (indistinguishable from black curve). (B) R_{pore} = 1 MΩ, R_{ct} = 10 KΩ, C_{dl} = 23.8 μF; (black) C_{mem} = 12.2 μF, (red) C_{mem} = 122 μF, (blue) C_{mem} = 1.22 μF. (C) R_{pore} = 1 MΩ, C_{mem} = 12.2 μF, C_{dl} = 23.8 μF; (black) R_{ct} = 10 KΩ, (red) R_{ct} = 1 KΩ, (blue) R_{ct} = 100 KΩ. (D) R_{pore} = 1 MΩ, C_{mem} = 12.2 μF, R_{ct} = 10 KΩ; (black) C_{dl} = 23.8 μF, (red) C_{dl} = 238 μF, (blue) C_{dl} = 2.38 μF. Note that both peak current and time depend on R_{pore}, R_{ct}, C_{mem}, and C_{dl}. Larger capacitance values result in slower current decays, as expected.

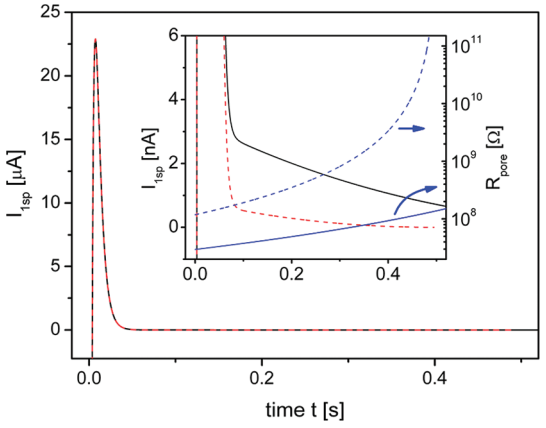

Figure 4. $I_{1sp}(t)$ transients employing a time-dependent R_{pore}, for two different initial pore diameters of 100 nm (black, solid) and 50 nm (red, dashed). At short times, the two transients seem to be identical and are relatively insensitive to the difference in R_{pore}. Inset: Magnified view of the low-current region with focus on longer times. Blue: R_{pore} as a function of time for the two cases (logarithmic scale). I_{1sp} now decays much slower and is given by eq 3 or eq 3a, if $R_s \ll R_{ct}$, R_{pore}.

size control by ion-current-controlled feedback somewhat difficult. Nevertheless, determining the deposition charge in real-time may offer an additional control parameter, especially when the deposition conditions around the nanopore are known.

Main Conclusions. Electrochemical reactions, such as electrodeposition or electrosynthesis, altering R_{pore} and R_{ct} can readily be incorporated into the model presented here. Simulation results are in line with available experimental data around the fabrication of metallic nanopores using bipotentiostatic electrodeposition, supporting its validity. To this end, simulations indicate that absolute size control based on ion current monitoring is challenging with the pore current being dependent on subtle details of the current distribution in the cell.

Determining the Pore Conductance—Ramping the Potential WE1. In a two-electrode nanopore device, a linear voltage sweep is used to determine the pore resistance from the slope of the current−voltage curve. In the presence of additional electrodes (or more generally current sources), however, the relation between R_{pore} and I_{1sp} no longer exists (see above) and a more detailed analysis is required.

We employ eqs 1 and 2, but now with $\tilde{E}_{1CR} = E_{1CR_0}/s + \nu/s^2$ and $\tilde{E}_{2CR} = E_{2CR}/s$ for $E_{1CR} = E_{1CR_0} + \nu t$ and E_{2CR} = constant, respectively. E_{1CR_0} is the initial potential of WE1 at the beginning of the potential sweep relative to CR, ν the scan rate [V/s]. In the time domain, the current I_{1sp}(for long t) is

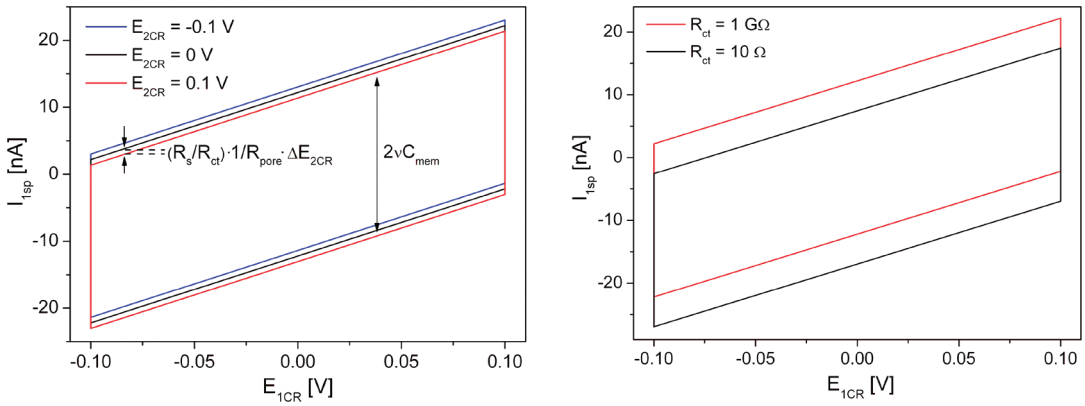

Figure 5. Simulated (cyclic) $I_{1sp}(E_{1CR})$ curves. Left: $E_{2CR} = -0.1$ V, 0 V, and +0.1 V (top to bottom), according to eq 9. Capacitive current and offset due to E_{2CR} are indicated. $R_s = 100\Omega$, $R_{ct} = 1000\ \Omega$, $R_{pore} = 10$ MΩ, $C_{mem} = 122$ nF, $C_{dl} = 23.8\ \mu$F, $\nu = 0.1$ V/s. (Right) Effect of R_{ct} as indicated, $R_{ct} = 1$ GΩ (red, top) and 10 Ω (black, bottom). $R_s = 100\ \Omega$, $R_{pore} = 10$ MΩ, $C_{mem} = 122$ nF, $C_{dl} = 23.8\ \mu$F, $\nu = 0.1$ V/s.

$$I_{1sp}(t) = \frac{R_{ct} + 2R_s}{5R_s^2 + (3R_{ct} + 2R_{pore})R_s + R_{pore}R_{ct}}(E_{1CR_0} + \nu t) - \frac{R_s}{5R_s^2 + (3R_{ct} + 2R_{pore})R_s + R_{pore}R_{ct}}E_{2CR} + \frac{(R_{ct} + 2R_s)^2 R_{pore}^2 c_{mem} + R_s^2 R_{ct}^2 c_{dl}}{5R_s^2 + (3R_{ct} + 2R_{pore})R_s + R_{pore}R_{ct}} \quad (9)$$

Several observations are important from an experimental point of view:

- The slope of the $I_{1sp}(E_{1CR})$ curve, which is typically used to determine the pore conductance, is the prefactor of $(E_{1CR_0} + \nu t)$ and depends on R_s, R_{ct}, and R_{pore}. However, as long as $R_{pore} \gg R_s$, this simplifies to $1/R_{pore}$, for both perfectly polarizable ($R_{ct} \to \infty$) and nonpolarizable ($R_{ct} \to 0$) electrodes WE2. Note that, according to eq 3, the steady-state current $I_{1sp}(t)_{ss}$ does *not* provide a direct measure for $1/R_{pore}$.
- The current offset at $E_{1CR} = 0$ V is dependent on E_{2CR}. For $R_{pore} \gg R_s$ and $R_{ct} \to 0$, this intercept changes by $1/(2R_{pore})$ per volt applied to E_{2CR}, allowing for an additional estimate of R_{pore}, *cf.* above. Given that R_{pore} is typically in the 100 MΩ-range, the current offset is relatively small and on the order of 10s nA. In the opposite limit, R_{pore}, $R_{ct} \gg R_s$, the intercept changes by $(R_s/R_{ct})(1/R_{pore})$ per volt applied to E_{2CR}. Thus, if R_{pore} is known from the gradient of I_{1sp} *versus* E_{1CR}, the intercept provides an estimate of R_{ct}.
- The actual capacitive current is the difference in $I_{1sp}(E_{1CR})$ between the forward and the reverse scan at given E_{1CR}, which equals to

$$2\frac{(R_{ct} + 2R_s)^2 R_{pore}^2 c_{mem} + R_s^2 R_{ct}^2 c_{dl}}{5R_s^2 + (3R_{ct} + 2R_{pore})R_s + R_{pore}R_{ct}}$$

Again, if $R_{pore} \gg R_s$, and C_{dl} and C_{mem} are both in the nanoFarad to microFarad range, the capacitive current is dominated by C_{mem}, namely equal to $2C_{mem}\nu$, for $R_{ct} \to 0$ and $R_{ct} \to \infty$. Perhaps somewhat surprisingly, C_{dl} does not feature prominently in this respect.

These effects are illustrated in Figure 5 below, for variations in E_{2CR} (left) and R_{ct} (right). Both parameters result in a (vertical) shift of the $I_{1sp}(E_{1CR})$ curve, since they affect the current from WE2 injected into or drawn from the cell. However, the slope is still $1/R_{pore}$ in all cases, as predicted above.

Hence, experimentally observed current offsets $I_{1sp}(E_{1CR} = 0\ \text{V}) \neq 0$ may be caused by additional current sources in the cell, including actively controlled electrodes or otherwise electrochemically active (*i.e.*, dissolving or corroding) surfaces. Liquid junction potentials may be another source, which can, however, be minimized by experimental design.

What Happens When We Ramp the Potential at WE2 Instead?

The derivation of $I_{1sp}(t)$ is analogous to the previous case, except that now $\tilde{E}_{1CR} = E_{1CR}/s$ and $E_{2CR} = ((E_{2CR_0})/s) + \nu/s^2$ for E_{1CR} = constant and $E_{2CR} = E_{2CR_0} + \nu t$. One expects similar expressions as in the previous section, but there are subtle differences, in terms of both the capacitive current and the slope of the $I_{1sp}(E_{2CR})$ curve. For long t, one obtains

$$I_{1sp} = (t) = \frac{R_{ct} + 2R_s}{5R_s^2 + (3R_{ct} + 2R_{pore})R_s + R_{pore}R_{ct}}E_{1CR} - \frac{R_s}{5R_s^2 + (3R_{ct} + 2R_{pore})R_s + R_{pore}R_{ct}}(E_{2CR_0} + \nu t) - \frac{(R_{pore} + 3R_s)R_s R_{ct}^2 C_{dl} + (R_{ct} + 2R_s)R_s R_{pore}^2 C_{mem}}{5R_s^2 + (3R_{ct} + 2R_{pore})R_s + R_{pore}R_{ct}}\nu \quad (10)$$

I_{1sp} decreases with increasing E_{2CR}, which is in-line with the notion above that an increase in E_{2CR} decreases the potential drop across the membrane, E_{1sp}. Since all solution resistances are taken to be the same and equal to R_s, the effective potential modulation at sp is at most $^1/_2E_{2CR}$ (for $R_{ct} \to 0$). Accordingly, the slope of the $I_{1sp}(E_{2CR})$ trace is equal to $-1/(2R_{pore})$ for $R_{pore} \gg R_s$ and $R_{ct} \to 0$, and $-R_s/(R_{ct}R_{pore})$ for R_{ct}, $R_{pore} \gg R_s$. The

latter emerges from the fact that, at large R_{ct}, most of E_{2CR} drops between sp and WE2, and not between CR and sp, as in the previous case.

As previously, the magnitude of the capacitive current depends on R_{ct}. Provided that C_{dl} and C_{mem} are again in the nanoFarad to microFarad range, the capacitive current equals νC_{mem} for $R_{pore} \gg R_s$ and $R_{ct} \rightarrow 0$ (perfectly nonpolarizable electrode WE2), and

$$2\nu\frac{R_s}{R_{pore}}C_{dl}$$

for $R_{pore} \gg R_s$ and $R_{ct} \rightarrow \infty$ (perfectly polarizable electrode WE2). In both limits, the capacitive current for the E_{2CR} sweep differs from the equivalent expressions in the previous section, implying that suitable potential modulation schemes for both electrodes WE1 and WE2 can be employed to estimate the impedance characteristics of the nanopore sensor.

Main Conclusions. Linear potential sweeps are a standard tool for assessing the operational state of a nanopore sensor. The observed currents, however, depend on how the potential modulation is applied. When ramping E_{1CR}, the slope of the current−voltage curve generally depends on R_s, R_{ct}, and R_{pore}. It is equal to $1/R_{pore}$ if $R_{pore} \gg R_s$ and thus remains a suitable means of estimating the pore geometry under typical experimental conditions. On the other hand, a sweep in E_{2CR} yields a current−voltage trace, whose slope directly depends on the solution resistance ratio between CR, sp, and WE2. This is difficult to determine experimentally and thus does not appear to be a reliable way to determine R_{pore}. The intercept at $I_{1sp}(E = 0)$ in the respective current−voltage sweeps depend on R_{ct}; and in combination with the slope may offer a way to estimate the actual charge transfer characteristics of WE2 *in situ*. Under relevant experimental conditions, the capacitive current depends on C_{mem} only in a E_{1CR}-sweep, whereas the situation is more complicated for a E_{2CR}-sweep, depending on R_{ct}.

Impedance Spectroscopy at the Nanopore—Applying an AC Modulation to WE2. AC modulation of the potential at WE2 has several interesting prospects, including local impedance spectroscopy and applications in biosensing. To this end, Aksimentiev *et al*. have suggested that a sinusoidal modulation can enhance the specificity of the nanopore sensor with regards to different short oligonucleotides.[38] However, as will be shown below, the coupling between the local electric field at the nanopore and the potential applied to WE2 again depends on R_{ct} in a nontrivial way.

Deriving the expressions for this case is rather cumbersome, even if short-lived transients are neglected for sufficiently long times. On the other hand, the variation in frequency and amplitude of $E_{2CR}(t)$ offers additional features with a view on analyzing the impedance behavior of the nanopore sensor. With a view on single biomolecule translocation studies, the frequency dependence of E_{1sp} is of particular importance, as the potential drop across the membrane governs the driving force for biopolymer translocation through the nanopore. Moreover, the phase angle between $E_{2CR}(t)$ and $E_{1sp}(t)$ can vary significantly, depending on the electric characteristics of the nanopore sensor cell and the excitation frequency. Hence, a detailed understanding of the sensor performance is central to using local potential modulation for single-biopolymer analysis, such as DNA fragment sizing or sequence analysis.

In accordance with the potential-time relations given above, the equivalent expressions in Laplace space are $\tilde{E}_{1CR} = E_{1CR}/s$ and $E_{2CR} = E_{2CR_0}/s + \Delta E_{2CR}(\omega/(\omega^2 + s^2))$. E_{1sp} already holds interesting features and will be considered explicitly first. After solving eq 1 and inverse Laplace transform, $E_{1sp}(t)$ is given by

$$E_{1sp}(t) = \frac{(R_{pore}+2R_S)(R_{ct}+2R_S)}{5R_S{}^2+(R_{ct}+2R_S)R_{pore}+3R_SR_{ct}}E_{1CR} - \frac{R_{pore}+2R_S}{5R_S{}^2+(R_{ct}+2R_S)R_{pore}+3R_SR_{ct}}E_{2CR}$$
$$- R_S\Delta E_{2CR}\left\{\frac{(4\omega^2R_S{}^2K_1{}^2+(R_{pore}+2R_S)^2)(\omega^2K_1{}^2+1)}{2S\omega^4R_S{}^4K_1{}^2K_2{}^2+[(2R_{pore}+5R_S)^2K_1{}^2+2R_{ct}R_{pore}K_1K_2+(3R_{ct}+5R_S)^2K_1{}^2]R_S{}^2\omega^2+(5R_S{}^2+(R_{ct}+2R_S)R_{pore}+3R_SR_{ct})^2}\right\}^{1/2}\sin(\omega t+\Phi(\omega)) \quad (11)$$

K_1 and K_2 are given by $R_{ct}C_{dl}$ and $R_{pore}C_{mem}$, respectively. $\Phi(\omega)$ is the phase angle between the excitation $E_{2CR}(t) = E_{2CR_0} + \Delta E_{2CR}\sin(\omega t)$ and the local potential difference between sp and WE1, $E_{1sp}(t)$. Note that eq 11 converts into eq 3 for $\Delta E_{2CR} = 0$, as expected.

$$\Phi(\omega) = \text{atan}\left(\frac{(6R_{ct}K_2 - R_{pore}K_1)R_3{}^2K_1{}^2K_2{}^2\omega^2+(R_{pore}+2R_s)R_{ct}K_1 - (R_{ct}+R_s)R_{pore}R_sK_2}{K_s}\omega\right) \quad (12)$$

$$K_3 = 10\omega^4R_s{}^3K_1{}^2K_2{}^2+[(2R_{pore}+5R_s)(R_{pore}+2R_s)K_1{}^2+R_{ct}R_{pore}K_1K_2+2R_s(3R_{ct}+5R_s)K_s{}^2]R_s\omega^2$$
$$+[(3R_{ct}+5R_s)R_s+(R_{ct}+2R_s)R_{pore}](R_{pore}+2R_S)$$

As before, the Laplace transform of eq 11 is the new input function to eq 2, which finally yields the current I_{1sp} between sp and WE1.

$$I_{1sp}(t) = \frac{(R_{ct}+2R_S)}{5R_S^2+(R_{ct}+2R_S)R_{pore}+3R_SR_{ct}}E_{1CR} - \frac{R_S}{5R_S^2+(R_{ct}+2R_S)R_{pore}+3R_SR_{ct}}E_{2CR}$$

$$-2R_S\Delta E_{2CR}\left\{\frac{(K_1^2\omega^2+1)(K_2^2\omega^2+1)}{2S\omega^4R_S^4K_1^2K_2^2+[(2R_{pore}+5R_S)^2K_1^2+2R_{ct}R_{pore}K_1K_2+(3R_{ct}+5R_S)^2K_2^2]R_S^2\omega^2+(5R_S^2+(R_{ct}+2R_S)R_{pore}+3R_SR_{ct})^2}\right\}^{1/2}$$

$$\times\sin(\omega t+\Phi_2(\omega)) \quad (13)$$

where $\Phi_2(\omega)$ is now the phase angle between $E_{2CR}(t)$ and $I_{1sp}(t)$.

$$\Phi_2(\omega) = \operatorname{atan}\left(\frac{(3R_{ct}K_2+2R_{pore}K_1)R_sK_1K_2\omega^2+(R_{pore}+3R_s)R_{ct}K_1+(R_{ct}+2R_s)R_{pore}K_2}{5R_s^2K_1^2K_2^2\omega^4+[(2R_{pore}+5R_s)R_sK_1^2-R_{ct}R_{pore}K_1K_2+(3R_{ct}+5R_s)R_sK_2^2]\omega^2+(R_{pore}+3R_s)R_{ct}+(2R_{pore}+5R_s)R_s}\omega\right) \quad (14)$$

Figure 6 shows the effect of the AC modulation at WE2 on the potential drop across the membrane, E_{1sp}, as well as the frequency dependence of the phase angle Φ, according to eq 12. Note that a high positive potential at WE2 counteracts a potential drop across the membrane, so the nominal value of the phase angle in fact relates a *maximum* in E_{2CR} to a *minimum* in E_{1sp}.

Note that in Figure 6 the modulation amplitude of E_{1sp} is reduced significantly relative to the excitation amplitude, which is again important with a view on using local AC modulation for biopolymer translocation control. The relative decrease depends on R_{ct} and R_s, as they affect the potential drop between WE2 and CR, and thus between WE1 and sp, *cf.* Figure 1B. More quantitatively, this relation emerges from the amplitude term in eq 11, which—after normalization to ΔE_{2CR}—is plotted Figure 7 for different values of R_{ct}. A number of observations are worth noting regarding the limiting behavior of the nanopore device, in terms of R_{ct} and ω. In the high-frequency limit, $\Delta E_{1sp}/\Delta E_{2CR} \rightarrow {}^2/_5$, so the local potential modulation E_{1sp} is always only 40% of the initial excitation (given the approximations made here). This value is also independent of R_{ct} and R_{pore}, since both resistances are "shorted out" by the capacitances C_{dl} and C_{mem} at high frequencies. In the low-frequency limit this is not the case: Provided that $R_{pore} \gg R_s$, one obtains $\Delta E_{1sp}/\Delta E_{2CR} \rightarrow R_s/(R_{ct}+2R_s)$, which is zero for $R_{ct} \rightarrow \infty$ (perfectly polarizable electrode WE2), since the entire potential drop occurs at R_{ct} and in between sp and WE2. In the opposite limit of $R_{ct} \rightarrow 0$ (perfectly nonpolarizable electrode), $\Delta E_{1sp}/\Delta E_{2CR} \rightarrow {}^1/_2$ corresponding to an equal potential drop at the two solution resistances between WE2 and CR.

More generally (and realistically), the solution resistances are not all equal, and in order to maximize the effect of $E_{2CR,AC}$ on E_{1sp}, the cell design needs to be such that $R_{s2'} \ll R_{s2}$.

Finally, we illustrate the effect of $E_{2CR}(t)$ (black, dashed line) on $E_{1sp}(t)$ (red, dash-dot) and $I_{1sp}(t)$ (black, solid) at different linear frequencies of 10 and 100 Hz in Figure 8 (left). The panel on the right-hand side shows the phase angles Φ (blue, dash-dot) and Φ_2 (black, solid), as well as the difference $\Phi_2 - \Phi$ (red, dashed) (see figure caption for further details).

First, as discussed above and shown in Figure 7, the amplitude of E_{1sp} relative to E_{2CR} depends on frequency and is larger for 100 Hz than for 10 Hz (R_{ct} = 10 kΩ). Due to the change in Φ and Φ_2, the exact relation between E_{2CR}, E_{1sp}, and I_{1sp} also varies, rendering the precise control of ion and biopolymer transport through the nanopore more difficult. A thorough characterization of the cell impedance should thus precede any biopolymer translocation experiments.

Table 1 summarizes the limiting cases for $R_{ct} \rightarrow 0$ and $R_{ct} \rightarrow \infty$ in the low and high frequency limits, respectively. If R_{ct} is small, say due to a fast interfacial reaction, efficient mass transport toward the electrode surface or a large electrode area, the limit of $\omega \rightarrow 0$ corresponds to adding another DC voltage ΔE_{2CR} to E_{2CR}, and thus to some degree also to E_{1sp} (*i.e.*, ΔE_{2CR} drops in accordance with the solution resistance). In the opposite limit of $\omega \rightarrow \infty$, ΔE_{2CR} also affects E_{1sp}, but now the current I_{1sp} is mainly determined by the solution resistances and usually large with R_s typically in the 100 Ω range; the impedance of the capacitive elements goes to zero. Even if the amplitude of the potential modulation is small, say 0.005 V, the condition $R_{pore} \gg R_s$ implies that the AC part of I_{1sp} is orders of magnitude larger than the DC components, dominating the overall current response.

For large $R_{ct} \rightarrow \infty$ and $\omega \rightarrow 0$, the phase angles are 90°, but note that in this limit the AC components of E_{1sp} and I_{1sp} drop to zero. This is expected, since under these conditions no charge can be transferred across the solution/WE2 interface, where also the entire potential drop between WE2 and CR occurs. This is also the reason why E_{2CR} does not affect E_{1sp} in this limit.

At high frequencies, $\omega \rightarrow \infty$, C_{dl} short-circuits R_{ct} and E_{2CR} does affect the potential distribution in the cell

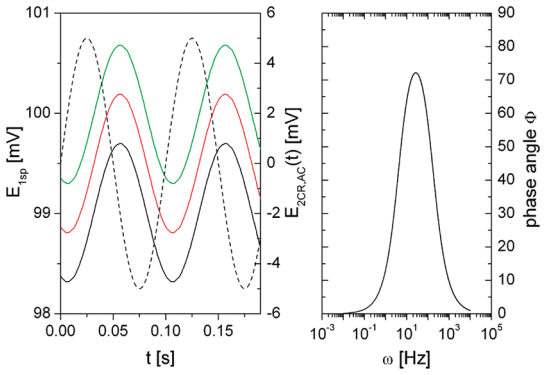

Figure 6. (Left) Modulation of E_{1sp} as a function of AC excitation $E_{2CR,AC}(t)$ (dashed line) at different DC potentials, top to bottom $E_{2CR} = -0.1$ V (green), 0 V (red), and +0.1 V (black). Frequency, $\omega = 2\pi 10$ Hz $\approx$ 63 Hz; amplitude, 10 mV (p−p). (Right) Phase angle Φ between E_{2CR} and E_{1sp}.

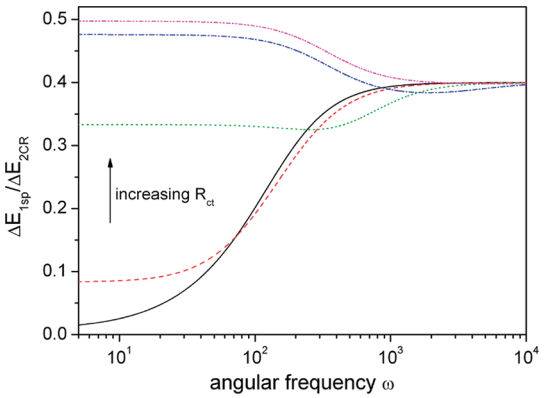

Figure 7. Simulation of $\Delta E_{1sp}/\Delta E_{2CR}(\omega)$ for increasing R_{ct} (top to bottom): 10 kΩ (magenta), 1 kΩ (blue), 100 Ω (green), 10 Ω (red), and 1Ω (black). $C_{dl} = 23.8\ \mu$F, $C_{mem} = 12.2\ \mu$F, $R_{pore} = 1$ MΩ, $R_s = 100$ Ω. At high frequencies the effect of R_{ct} is negligible, but at low frequencies $\Delta E_{1sp}/\Delta E_{2CR}(\omega)$ is strongly affected. Note that, at intermediate ω, the frequency dependence of $\Delta E_{1sp}/\Delta E_{2CR}(\omega)$ can be rather complex and difficult to predict without comprehensive electric characterization of the nanopore device.

again. The component of I_{1sp} is again unaffected by E_{2CR}, but the amplitude of the AC current is determined by R_s and ΔE_{2CR}. As before, this can be much larger than the DC contribution to the current and ultimately dominate the current detected at WE1.

Main conclusions. As shown previously, the potential drop across the membrane E_{1sp} depends on the potential applied to WE2 and the relative potential drops between CR, sp, and WE2. In AC modulation, however, the latter depends on the impedance of the capacitive elements, too, which are frequency-dependent. Since the potential drop across the membrane is often the dominating driving force for biopolymer translocation, a comprehensive impedance characterization of the nanopore sensor is needed. Interestingly in the high-frequency regime, the nanopore current is governed to a large extent by the solution resistance R_s with R_{pore} "shorted out" by C_{mem}., at least in the model circuit used here. Since R_s is typically small compared to R_{pore}, the corresponding current can be large.

Potential Modulation at WE2 in the Presence of Interfacial Reactions. Interfacial redox reactions on the surface of WE2 affect the current distribution in the electrochemical cell. The reaction rate and thus the associated Faradaic current is generally potential-dependent, and expected to vary during an AC voltage swing. In the following, we shall assume the presence of a generic redox couple, present in solution at equal concentrations, that undergoes oxidation/reduction at WE2 with a characteristic equilibrium redox potential E^0. We shall further assume that R_{ct} is governed by the surface reaction and not mass transport toward the surface.

So far R_{ct} was assumed to take particular values from very large to zero; however, its potential-dependence has so far been ignored. While this may be unimportant when the potential modulation of WE2 is small or when R_{ct} does not vary much relative to other sources of resistance in the cell, it is more relevant at large potentials or when R_{ct} is on the same order as R_s. Note that, even if full potential control is maintained, that is, the potential drop at the WE2/solution interface is unaffected by E_{1CR}, the latter contribution to I_{1sp} will still be affected by a change in R_{ct} (Figure 9, *cf.*, eq 10.

The potential dependence of R_{ct} can be written as in eq 15, implying that mass transport is not limiting the current (at WE2), *vide supra*.

$$R_{ct}^{-1} = \frac{n^z F^z}{RT} A_{el} \left[\alpha k_a^0 C_R^{surf} \exp\left(\frac{\alpha n F E}{RT}\right) + (1-\alpha) k_c^0 C_o^{surf} \exp\left(-\frac{(1-\alpha) n F E}{RT}\right) \right] \quad (15)$$

where n is the number of electrons transferred per redox event; F is Faraday's constant; R is the universal gas constant; T is the temperature; A_{el} is the electrode area; α is the transfer coefficient taken to be 0.5; k_a^0 and k_c^0 are potential-independent parts of the anodic and cathodic interfacial charge transfer rate constants, respectively; c_R^{surf}, c_O^{surf} are the surface concentration of reduced and oxidized species; E is the applied potential, relative to the equilibrium potential E^0 of the redox species involved in charge transfer (overpotential), $E = E_{2CR} - E^0$.

Compared to Figure 2, which shows the same plots of I_{1sp} for $R_{ct} = 0$ Ω and $R_{ct} \to \infty$, the current−voltage characteristics are qualitatively different. While relatively little happens around the redox potential of the hypothetical redox couple ($R_{ct} > R_s$), I_{1sp} changes rapidly when R_{ct} becomes smaller than R_s at larger overpotentials. Both oxidized and reduced redox species are present in solution, allowing for a significant steady-state current at high and low potentials, respectively. Nevertheless, I_{1sp} is still asymmetric with respect to E_{2CR} (due to $E^0 \neq 0$), which is reminiscent of diode-like behavior in electrostatically asymmetric conical pores.[35,39−41] Note, however, that the origin of the

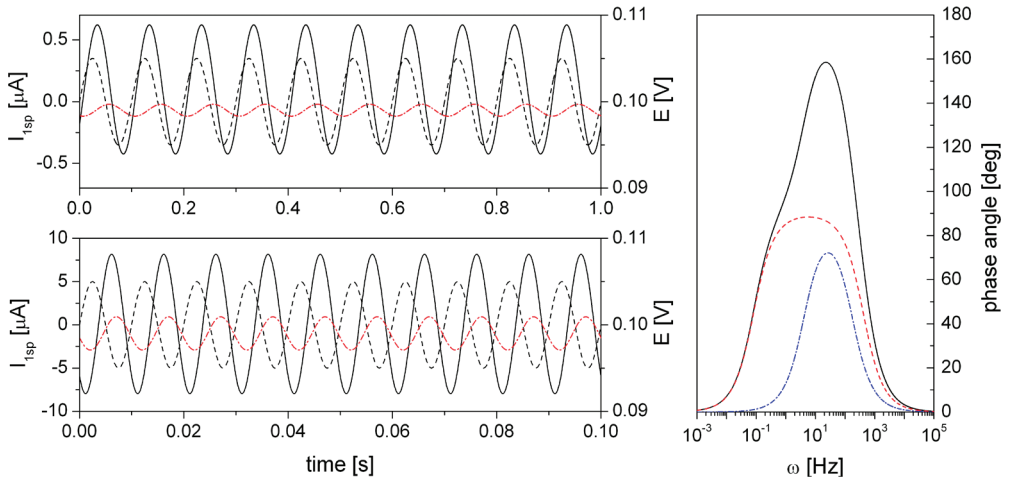

Figure 8. Simulated system responses in the domain (panels on the left) and phase angle (right panel) according to eqs 11 − 14. C_{mem} = 12.2 μF, C_{dl} = 23.8 μF, R_s = 100 Ω, R_{ct} = 10 kΩ, R_{pore} = 1 MΩ, E_{1CR} = 0.1 V, $E_{2CR,DC}$ = 0.1 V, amplitude: 0.01 V (p−p). (Left panels) Potential- and current−time traces for f = 10 Hz (top) and 100 Hz (bottom). Dashed (black) and dash-dotted (red) lines: $E_{1sp}(t)$ and $E_{2CR}(t)$, respectively (right axis). Solid (black) lines: $I_{1sp}(t)$ (left axis). (Right panel) Phase angle $\Phi_2(\omega)$ (black, solid) and $\Phi(\omega)$ (dash-dot, blue) and the difference between the two (dashed, red) corresponding to the phase angle between E_{1sp} and I_{1sp}.

TABLE 1. Comparison of Phase Angles, E_{1sp} and I_{1sp} in Different Limits of R_{ct} and ω

	$R_{ct} \to 0$		$R_{ct} \to \infty$	
	$\omega \to 0$	$\omega \to \infty$	$\omega \to 0$	$\omega \to \infty$
Φ	0	0	90°	0
Φ_2	0	0	90°	0
E_{1sp}	$-{}^1/_2\Delta E_{2CR}$ + DC DC = $E_{1CR} - {}^1/_2\Delta E_{2CR}$	$-{}^2/_5\Delta E_{2CR}$ + DC	DC part only DC = E_{1CR}	$-{}^1/_5\Delta E_{2CR}$ + DC
I_{1sp}	$-(1/(2R_{pore}))\Delta E_{2CR}$ + DC DC = $(1/(R_{pore}))(E_{1CR} - {}^1/_2\Delta E_{2CR})$	$-(1/(5R_s))\Delta E_{2CR}$ + DC	DC part only DC = $(1/(R_{pore}))E_{1CR}$	$-(1/(5R_s))\Delta E_{2CR}$ +DC

rectification effect is quite different here and simply rooted in the altered current distribution in the cell, rather than the modulation of the pore conductance itself. Accordingly, the asymmetry would increase if only one redox state was present in significant amounts.

In the case of small amplitude AC modulation on WE2, the potential dependence of R_{ct} will generally have a small effect on $I_{1sp}(t)$. Significant distortions of the sinusoidal response do occur however, when R_{ct} varies significantly around R_s during a voltage swing. This is because R_{ct} then has a significant effect on the local potential distribution at sp, which in turn affects the current across the pore. The effect is illustrated in Figure 10 based on eq 13 and a sinusoidal potential modulation on WE2 (linear frequency, 1 Hz; amplitude, 10 mV (p−p). R_{ct} in eq 15 then becomes time-dependent (E_{1CR} = 0.05 V; E_{2CR} = −0.25 V; ΔE_{2CR} = 0.1 V; E^0 = −0.01 V; all other parameters for R_{ct} as above) and varies from 70 to 3470 Ω.

Such current−time characteristics could potentially be exploited to fine-tune the electric driving force for biopolymer translocation and warrants further experimental investigation.

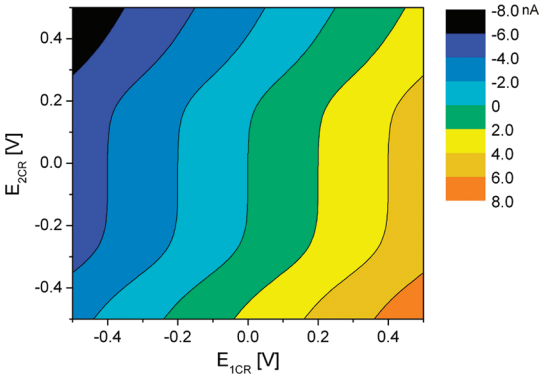

Figure 9. Contour plot of I_{1sp} as a function of E_{1CR} and E_{2CR}, based on eq 3, but with a potential-dependent R_{ct}, eq 15. E^0 = 0.05 V *vs* CR, $R_{ct}(E_{2CR} = E^0)$ = 26 kΩ, decreasing to ~1Ω at large E_{2CR}: n = 1, $k_a^0 = k_c^0 = 1 \times 10^{-3}$, $c_R^{surf} = c_O^{surf} = 1 \times 10^{-3}$, $A_{el} = 1 \times 10^{-5}$; T = 298 K. Note that the colors indicate current ranges, not constant current value (to which the contour lines correspond).

Main Conclusions. This section briefly considers the effect of a potential-dependent R_{ct} on the nanopore sensor performance. Interestingly, interfacial redox

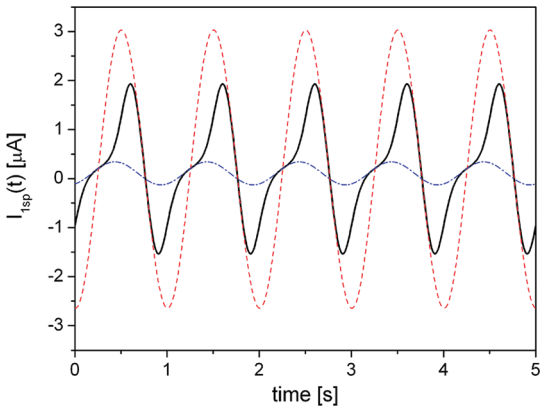

Figure 10. The effect of a potential-dependent R_{ct} on the shape of $I_{1sp}(t)$. Significant distortions of the sinusoidal excitation occur, when R_{ct} is on the order of R_s: (black, solid line) $R_{ct}(t)$ varies from 70 Ω to 3470 Ω, according to eq 15; (red, dashed line) R_{ct} = 70 Ω; (blue, dash-dotted line) R_{ct} = 3470 Ω (further details are given in the text).

reactions can result in an apparent rectification of the current across the nanopore. This "pseudo-rectification" behavior is, however, rooted purely in the interfacial electron transfer kinetics and not in preferential ion transport.

In the case of small-amplitude AC modulation, the potential-dependence of R_{ct} is only a minor factor, unless $R_{ct} \approx R_s$. In the latter case, the impact on the pore current is notable, leading to significant distortions in pore current−time trace and in the electric field driving biopolymer translocation through the pore.

CONCLUSIONS

In summary, we have shown for a model three-electrode nanopore sensor device that the charge transfer characteristics of each electrode need to be taken into account for a full understanding of the sensor performance. While the exact circuit representation of a nanopore sensor will depend on the actual cell design, including electrode geometries, distances, materials *etc.*, and may need adaptation, the main conclusions from our study remain valid. On a fundamental level, the role of R_{ct} is important for the interpretation of ion current and pore conductance data, for example, to extract the pore geometry, as the direct connection between R_{pore} and ion current is generally lost, whenever additional current sources are present in the cell. Our model provides guidelines as to when the charge transfer characteristics of additional electrodes are expected to be important for device performance. Moreover, the consequences extend to applications where precise control of biopolymer transport through the pore is required, for example in DNA fragment sizing or sequencing. With a view on local AC modulation of the translocation field, R_{ct} crucially affects the phase angle between the potential modulation at WE2 and the driving field across the membrane. Accordingly, the electric field strength at the pore may be large when the potential modulation is at a minimum, and vice versa. Finally, our simulations point to the fact that even at relatively low frequencies, the overall current is dominated by capacitive charging or ultimately by the relatively low solution resistance, rendering the detection of small nanopore conductance modulations rather difficult.

Ultimately, the model presented could readily be extended to include other electrode geometries or more than three electrodes, for example toward developing an understanding of four-electrode tunneling junction/nanopore devices for DNA sequencing applications.

METHODS

According to Kirchoff's First Rule, I_{1sp} must be equal to the sum of the currents between sp and CR, and sp and WE2, respectively.

$$I_{1sp} + I_{2sp} + I_{spCR} = 0 \tag{16}$$

The currents through each branch are governed by their admittance Y and the potential difference between sp and the respective electrode. Note, however, that the potential at sp, E_{sp}, is dependent on I_{1sp}, I_{2sp}, and I_{spCR}. Hence

$$\tilde{I}_{spCR} = Y_{spCR}\tilde{E}_{spCR} = \frac{1}{R_{s2}}\tilde{E}_{spCR} \tag{17a}$$

$$\tilde{I}_{1sp} = Y_{1sp}\tilde{E}_{1sp} = \frac{1 + sC_{mem}R_{pore}}{R_{pore} + (R_{s1} + R''_{s2})(1 + sC_{mem}R_{pore})}\tilde{E}_{1sp} \tag{17b}$$

$$\tilde{I}_{2sp} = Y_{2sp}\tilde{E}_{2sp} = \frac{1 + sC_{dl}R_{ct}}{R_{ct} + R_{s2}(1 + sC_{dl}R_{ct})}\tilde{E}_{2sp} \tag{17c}$$

where s is the (imaginary part of the) Laplace parameter, $s = i\omega$. $\tilde{E}_{1CR}$ is the sum of the potential differences between sp and CR (in Laplace space), and WE1 and sp, respectively ($\tilde{E}_{1CR} = \tilde{E}_{spCR} + \tilde{E}_{1sp}$). An analogous expression also applies to $\tilde{E}_{2CR}$. In combination with eqs 16 and 17, this yields

$$\tilde{E}_{spCR} = Y_{1sp}\tilde{E}_{1CR} + Y_{2sp}\frac{\tilde{E}_{2CR}}{Y_{spCR} + Y_{1sp} + Y_{2sp}} = \tilde{E}_{1CR} - \tilde{E}_{1sp} \tag{18}$$

and equation 1 for $\tilde{E}_{1sp}$.

This expression represents an important result, as it stands for the potential difference between WE1 and sp and thus the driving force behind ion and biopolymer transport through the nanopore. The current measured at WE1, $\tilde{I}_{1sp}$, can readily be calculated using eq 1 as the new input function in eq 2.

Different input functions for E_{1CR} and E_{2CR} can now be entered into eq 1; I_{1sp} in the time-domain is obtained from eq 2 after inverse Laplace transform. The resulting expressions are in some cases relatively cumbersome and, in order to keep the mathematical expressions reasonably simple, all solution resistances will be taken to be numerically equal (corresponding to choosing a particular cell and electrode geometry) and given by R_s. This has only minor (quantitative) effects on the

final result, for example for $R_{ct} \rightarrow 0$ and constant E_{1CR} and E_{2CR}, when the potential drop between sp and WE2 is always exactly $^1/_2E_{2CR}$, rather than a fraction $R_{s2}/(R_{s2} + R_{s2'})$.

Acknowledgment. The author would like to thank A. Kornyshev, J. B. Edel and A. Ivanov for reading the manuscript and for helpful suggestions and comments.

Supporting Information Available: The effect of R_{ct} on I_{1sp} (electric model circuit); comparison between numerical and analytical simulation results. This material is available free of charge *via* the Internet at http://pubs.acs.org.

REFERENCES AND NOTES

1. Li, J.; Stein, D.; McMullan, C.; Branton, D.; Aziz, M. J.; Golovchenko, J. A. Ion-Beam Sculpting at Nanometre Length Scales. *Nature* **2001**, *412*, 166–169.
2. Meller, A.; Nivon, L.; Brandin, E.; Golovchenko, J.; Branton, D. Rapid Nanopore Discrimination between Single Polynucleotide Molecules. *Proc. Natl. Acad. Sci. U.S.A.* **2000**, *97*, 1079–1084.
3. Garaj, S.; Hubbard, W.; Reina, A.; Kong, J.; Branton, D.; Golovchenko, J. A. Graphene as a Subnanometre Trans-Electrode Membrane. *Nature* **2010**, *467*, 190–U73.
4. Akeson, M.; Branton, D.; Kasianowicz, J. J.; Brandin, E.; Deamer, D. W. Microsecond Time-Scale Discrimination among Polycytidylic Acid, Polyadenylic Acid, and Polyuridylic Acid as Homopolymers or as Segments within Single RNA Molecules. *Biophys. J.* **1999**, *77*, 3227–3233.
5. Meller, A.; Nivon, L.; Branton, D. Voltage-driven DNA Translocations through a Nanopore. *Phys. Rev. Lett.* **2001**, *86*, 3435–3438.
6. Merchant, C. A; Healy, K.; Wanunu, M.; Ray, V.; Peterman, N.; Bartel, J.; Fischbein, M. D.; Venta, K.; Luo, Z. T.; Johnson, A. T. C.; *et al.* DNA Translocation through Graphene Nanopores. *Nano Lett.* **2011**, *10*, 2915–2921.
7. Schneider, G. F.; Kowalczyk, S. W.; Calado, V. E.; Pandraud, G.; Zandbergen, H. W.; Vandersypen, L. M. K.; Dekker, C. DNA Translocation through Graphene Nanopores. *Nano Lett.* **2010**, *10*, 3163–3167.
8. Dekker, C. Solid-State Nanopores. *Nat. Nanotechnol.* **2007**, *2*, 209–215.
9. Keyser, U. F.; Koeleman, B. N.; Van Dorp, S.; Krapf, D.; Smeets, R. M. M.; Lemay, S. G.; Dekker, N. H.; Dekker, C. Direct Force Measurements on DNA in a Solid-State Nanopore. *Nat. Phys.* **2006**, *2*, 473–477.
10. Storm, A. J.; Chen, J. H.; Zandbergen, H. W.; Dekker, C. Translocation of Double-Strand DNA through a Silicon Oxide Nanopore. *Phys. Rev. E* **2005**, *71*, 051903.
11. Storm, A. J.; Storm, C.; Chen, J. H.; Zandbergen, H.; Joanny, J. F.; Dekker, C. Fast DNA Translocation through a Solid-State Nanopore. *Nano Lett.* **2005**, *5*, 1193–1197.
12. Howorka, S.; Cheley, S.; Bayley, H. Sequence-Specific Detection of Individual DNA Strands Using Engineered Nanopores. *Nat. Biotechnol.* **2001**, *19*, 636–639.
13. Howorka, S.; Movileanu, L.; Braha, O.; Bayley, H. Kinetics of Duplex Formation for Individual DNA Strands within a Single Protein Nanopore. *Proc. Natl. Acad. Sci. U.S.A.* **2001**, *98*, 12996–13001.
14. Vercoutere, W.; Winters-Hilt, S.; Olsen, H.; Deamer, D.; Haussler, D.; Akeson, M. Rapid Discrimination among Individual DNA Hairpin Molecules at Single-Nucleotide Resolution Using an Ion Channel. *Nat. Biotechnol.* **2001**, *19*, 248–252.
15. Vercoutere, W. A.; Akeson, M.; Olsen, H.; Deamer, D. W. Analysis of Hairpin Structures within Single DNA Molecules Using a Nanopore Detector. *Biophys. J.* **2000**, *78*, 402A–402A.
16. Ambjornsson, T.; Apell, S. P.; Konkoli, Z.; Di Marzio, E. A.; Kasianowicz, J. J. Charged Polymer Membrane Translocation. *J. Chem. Phys.* **2002**, *117*, 4063–4073.
17. Kasianowicz, J. J. Nanopores—Flossing with DNA. *Nat. Mater.* **2004**, *3*, 355–356.
18. Branton, D.; Deamer, D. W.; Marziali, A.; Bayley, H.; Benner, S. A.; Butler, T.; Di Ventra, M.; Garaj, S.; Hibbs, A.; Huang, X. H.; *et al.* The Potential and Challenges of Nanopore Sequencing. *Nat. Biotechnol.* **2008**, *26*, 1146–1153.
19. Deamer, D. W.; Akeson, M. Nanopores and Nucleic Acids: Prospects for Ultrarapid Sequencing. *Trends Biotechnol.* **2000**, *18*, 147–151.
20. Zwolak, M.; Di Ventra, M. Colloquium: Physical Approaches to DNA Sequencing and Detection. *Rev. Mod. Phys.* **2008**, *80*, 141–165.
21. Howorka, S.; Siwy, Z. Nanopore Analytics: Sensing of Single Molecules. *Chem. Soc. Rev.* **2009**, *38*, 2360–2384.
22. Schoch, R. B.; Han, J. Y.; Renaud, P. Transport Phenomena in Nanofluidics. *Rev. Mod. Phys.* **2008**, *80*, 839–883.
23. Ayub, M.; Ivanov, A.; Hong, J.; Kuhn, P.; Instuli, E.; Edel, J. B.; Albrecht, T. Precise Electrochemical Fabrication of sub-20 nm Solid-State Nanopores for Single-Molecule Biosensing. *J. Phys. Condens. Mater.* **2010**, *22*, 454128.
24. Ayub, M.; Ivanov, A.; Instuli, E.; Cecchini, M.; Chansin, G.; McGilvery, C.; Hong, J. G.; Baldwin, G.; McComb, D.; Edel, J. B.; Albrecht, T. Nanopore/Electrode Structures for Single-Molecule Biosensing. *Electrochim. Acta* **2010**, *55*, 8237–8243.
25. Chun, K. Y.; Mafe, S.; Ramirez, P.; Stroeve, P. Protein Transport through Gold-Coated, Charged Nanopores: Effects of Applied Voltage. *Chem. Phys. Lett.* **2006**, *418*, 561–564.
26. Nishizawa, M.; Menon, V. P.; Martin, C. R. Metal Nanotubule Membranes with Electrochemically Switchable Ion-Transport Selectivity. *Science* **1995**, *268*, 700–702.
27. Gierhart, B. C.; Howitt, D. G.; Chen, S. J.; Zhu, Z.; Kotecki, D. E.; Smith, R. L.; Collins, S. D. Nanopore with Transverse Nanoelectrodes for Electrical Characterization and Sequencing of DNA. *Transducers '07 Eurosens. XXI, Dig. Tech. Pap.* **2007**, *1, 2*, U203–U204.
28. Ivanov, A. P.; Instuli, E.; McGilvery, C. M.; Baldwin, G.; McComb, D. W.; Albrecht, T.; Edel, J. B. DNA Tunneling Detector Embedded in a Nanopore. *Nano Lett.* **2011**, *11*, 279–285.
29. Jiang, Z. J.; Mihovilovic, M.; Chan, J.; Stein, D. Fabrication of Nanopores with Embedded Annular Electrodes and Transverse Carbon Nanotube Electrodes. *J. Phys. Condens. Mater.* **2010**, *22*, 454114.
30. Krems, M.; Zwolak, M.; Pershin, Y. V.; Di Ventra, M. Effect of Noise on DNA Sequencing *via* Transverse Electronic Transport. *Biophys. J.* **2009**, *97*, 1990–1996.
31. Zwolak, M.; Di Ventra, M. Electronic Signature of DNA Nucleotides *via* Transverse Transport. *Nano Lett.* **2005**, *5*, 421–424.
32. Cervera, J.; Schiedt, B.; Neumann, R.; Mafe, S.; Ramirez, P. Ionic Conduction, Rectification, and Selectivity in Single Conical Nanopores. *J. Chem. Phys.* **2006**, *124*, 104706.
33. Ho, C.; Qiao, R.; Heng, J. B.; Chatterjee, A.; Timp, R. J.; Aluru, N. R.; Timp, G. Electrolytic Transport through a Synthetic Nanometer-Diameter Pore. *Proc. Natl. Acad. Sci. U.S.A.* **2005**, *102*, 10445–10450.
34. Karnik, R.; Fan, R.; Yue, M.; Li, D. Y.; Yang, P. D.; Majumdar, A. Electrostatic Control of Ions and Molecules in Nanofluidic Transistors. *Nano Lett.* **2005**, *5*, 943–948.
35. Siwy, Z. S. Ion-Current Rectification in Nanopores and Nanotubes with Broken Symmetry. *Adv. Funct. Mater.* **2006**, *16*, 735–746.
36. Zhang, Y. H.; Zhang, B.; White, H. S. Electrochemistry of Nanopore Electrodes in Low Ionic Strength Solutions. *J. Phys. Chem. B* **2006**, *110*, 1768–1774.
37. Chansin, G. A. T.; Mulero, R.; Hong, J.; Kim, M. J.; DeMello, A. J.; Edel, J. B. Single-Molecule Spectroscopy Using Nanoporous Membranes. *Nano Lett.* **2007**, *7*, 2901–2906.
38. Sigalov, G.; Comer, J.; Timp, G.; Aksimentiev, A. Detection of DNA Sequences Using an Alternating Electric Field in a Nanopore Capacitor. *Nano Lett.* **2008**, *8*, 56–63.
39. Fulinski, A.; Kosinska, I.; Siwy, Z. Transport Properties of Nanopores in Electrolyte Solutions: The Diffusional Model and Surface Currents. *New J. Phys.* **2005**, *7*, 132.
40. Siwy, Z.; Fulinski, A. A Nanodevice for Rectification and Pumping Ions. *Am. J. Phys.* **2004**, *72*, 567–574.
41. Siwy, Z.; Kosinska, I. D.; Fulinski, A.; Martin, C. R. Asymmetric Diffusion through Synthetic Nanopores. *Phys. Rev. Lett.* **2005**, *94*, 048102.